Study of $\Upsilon(1s)$ Radiative Decays to $\gamma\pi^+\pi^-$ and γK^+K^-

UT Dallas Author(s):

Joseph M. Izen
Xinchou Lou

Citation:

Lees, J. P., V. Poireau, V. Tisserand, E. Grauges, et al. 2018. "Study of $\Upsilon(1S)$ radiative decays to $\gamma\pi^+\pi^-$ and γK^+K^-." Physical Review D 97(11): 112006-1 to 17, doi:10.1103/PhysRevD.97.112006

Study of $\Upsilon(1S)$ radiative decays to $\gamma\pi^+\pi^-$ and γK^+K^-

J. P. Lees,[1] V. Poireau,[1] V. Tisserand,[1] E. Grauges,[2] F. Giannuzzi,[3a] A. Palano,[3a,3b] G. Eigen,[4] D. N. Brown,[5] Yu. G. Kolomensky,[5] M. Fritsch,[6] H. Koch,[6] T. Schroeder,[6] C. Hearty,[7a,7b] T. S. Mattison,[7b] J. A. McKenna,[7b] R. Y. So,[7b] V. E. Blinov,[8a,8b,8c] A. R. Buzykaev,[8a] V. P. Druzhinin,[8a,8b] V. B. Golubev,[8a,8b] E. A. Kozyrev,[8a,8b] E. A. Kravchenko,[8a,8b] A. P. Onuchin,[8a,8b,8c] S. I. Serednyakov,[8a,8b] Yu. I. Skovpen,[8a,8b] E. P. Solodov,[8a,8b] K. Yu. Todyshev,[8a,8b] A. J. Lankford,[9] J. W. Gary,[10] O. Long,[10] A. M. Eisner,[11] W. S. Lockman,[11] W. Panduro Vazquez,[11] D. S. Chao,[12] C. H. Cheng,[12] B. Echenard,[12] K. T. Flood,[12] D. G. Hitlin,[12] J. Kim,[12] Y. Li,[12] T. S. Miyashita,[12] P. Ongmongkolkul,[12] F. C. Porter,[12] M. Röhrken,[12] Z. Huard,[13] B. T. Meadows,[13] B. G. Pushpawela,[13] M. D. Sokoloff,[13] L. Sun,[13,†] J. G. Smith,[14] S. R. Wagner,[14] D. Bernard,[15] M. Verderi,[15] D. Bettoni,[16a] C. Bozzi,[16a] R. Calabrese,[16a,16b] G. Cibinetto,[16a,16b] E. Fioravanti,[16a,16b] I. Garzia,[16a,16b] E. Luppi,[16a,16b] V. Santoro,[16a] A. Calcaterra,[17] R. de Sangro,[17] G. Finocchiaro,[17] S. Martellotti,[17] P. Patteri,[17] I. M. Peruzzi,[17] M. Piccolo,[17] M. Rotondo,[17] A. Zallo,[17] S. Passaggio,[18] C. Patrignani,[18,‡] H. M. Lacker,[19] B. Bhuyan,[20] U. Mallik,[21] C. Chen,[22] J. Cochran,[22] S. Prell,[22] A. V. Gritsan,[23] N. Arnaud,[24] M. Davier,[24] F. Le Diberder,[24] A. M. Lutz,[24] G. Wormser,[24] D. J. Lange,[25] D. M. Wright,[25] J. P. Coleman,[26] E. Gabathuler,[26,*] D. E. Hutchcroft,[26] D. J. Payne,[26] C. Touramanis,[26] A. J. Bevan,[27] F. Di Lodovico,[27] R. Sacco,[27] G. Cowan,[28] Sw. Banerjee,[29] D. N. Brown,[29] C. L. Davis,[29] A. G. Denig,[30] W. Gradl,[30] K. Griessinger,[30] A. Hafner,[30] K. R. Schubert,[30] R. J. Barlow,[31,§] G. D. Lafferty,[31] R. Cenci,[32] A. Jawahery,[32] D. A. Roberts,[32] R. Cowan,[33] S. H. Robertson,[34a,34b] R. M. Seddon,[34b] B. Dey,[35a] N. Neri,[35a] F. Palombo,[35a,35b] R. Cheaib,[36] L. Cremaldi,[36] R. Godang,[36,‖] D. J. Summers,[36] P. Taras,[37] G. De Nardo,[38] C. Sciacca,[38] G. Raven,[39] C. P. Jessop,[40] J. M. LoSecco,[40] K. Honscheid,[41] R. Kass,[41] A. Gaz,[42a] M. Margoni,[42a,42b] M. Posocco,[42a] G. Simi,[42a,42b] F. Simonetto,[42a,42b] R. Stroili,[42a,42b] S. Akar,[43] E. Ben-Haim,[43] M. Bomben,[43] G. R. Bonneaud,[43] G. Calderini,[43] J. Chauveau,[43] G. Marchiori,[43] J. Ocariz,[43] M. Biasini,[44a,44b] E. Manoni,[44a] A. Rossi,[44a] G. Batignani,[45a,45b] S. Bettarini,[45a,45b] M. Carpinelli,[45a,45b,¶] G. Casarosa,[45a,45b] M. Chrzaszcz,[45a] F. Forti,[45a,45b] M. A. Giorgi,[45a,45b] A. Lusiani,[45a,45c] B. Oberhof,[45a,45b] E. Paoloni,[45a,45b] M. Rama,[45a] G. Rizzo,[45a,45b] J. J. Walsh,[45a] L. Zani,[45a,45b] A. J. S. Smith,[46] F. Anulli,[47a] R. Faccini,[47a,47b] F. Ferrarotto,[47a] F. Ferroni,[47a,47b] A. Pilloni,[47a,47b] G. Piredda,[47a,*] C. Bünger,[48] S. Dittrich,[48] O. Grünberg,[48] M. Heß,[48] T. Leddig,[48] C. Voß,[48] R. Waldi,[48] T. Adye,[49] F. F. Wilson,[49] S. Emery,[50] G. Vasseur,[50] D. Aston,[51] C. Cartaro,[51] M. R. Convery,[51] J. Dorfan,[51] W. Dunwoodie,[51] M. Ebert,[51] R. C. Field,[51] B. G. Fulsom,[51] M. T. Graham,[51] C. Hast, W. R. Innes,[51,*] P. Kim,[51] D. W. G. S. Leith,[51] S. Luitz,[51] D. B. MacFarlane,[51] D. R. Muller,[51] H. Neal,[51] B. N. Ratcliff,[51] A. Roodman,[51] M. K. Sullivan,[51] J. Va'vra,[51] W. J. Wisniewski,[51] M. V. Purohit,[52] J. R. Wilson,[52] A. Randle-Conde,[53] S. J. Sekula,[53] H. Ahmed,[54] M. Bellis,[55] P. R. Burchat,[55] E. M. T. Puccio,[55] M. S. Alam,[56] J. A. Ernst,[56] R. Gorodeisky,[57] N. Guttman,[57] D. R. Peimer,[57] A. Soffer,[57] S. M. Spanier,[58] J. L. Ritchie,[59] R. F. Schwitters,[59] J. M. Izen,[60] X. C. Lou,[60] F. Bianchi,[61a,61b] F. De Mori,[61a,61b] A. Filippi,[61a] D. Gamba,[61a,61b] L. Lanceri,[62] L. Vitale,[62] F. Martinez-Vidal,[63] A. Oyanguren,[63] J. Albert,[64b] A. Beaulieu,[64b] F. U. Bernlochner,[64b] G. J. King,[64b] R. Kowalewski,[64b] T. Lueck,[64b] I. M. Nugent,[64b] J. M. Roney,[64b] R. J. Sobie,[64a,64b] N. Tasneem,[64b] T. J. Gershon,[65] P. F. Harrison,[65] T. E. Latham,[65] R. Prepost,[66] and S. L. Wu[66]

(The *BABAR* Collaboration)

[1]*Laboratoire d'Annecy-le-Vieux de Physique des Particules (LAPP), Université de Savoie, CNRS/IN2P3, F-74941 Annecy-Le-Vieux, France*
[2]*Universitat de Barcelona, Facultat de Fisica, Departament ECM, E-08028 Barcelona, Spain*
[3a]*INFN Sezione di Bari, I-70126 Bari, Italy*
[3b]*Dipartimento di Fisica, Università di Bari, I-70126 Bari, Italy*
[4]*University of Bergen, Institute of Physics, N-5007 Bergen, Norway*
[5]*Lawrence Berkeley National Laboratory and University of California, Berkeley, California 94720, USA*
[6]*Ruhr Universität Bochum, Institut für Experimentalphysik 1, D-44780 Bochum, Germany*
[7a]*Institute of Particle Physics, Vancouver, British Columbia V6T 1Z1, Canada*
[7b]*University of British Columbia, Vancouver, British Columbia V6T 1Z1, Canada*
[8a]*Budker Institute of Nuclear Physics SB RAS, Novosibirsk 630090, Russia*
[8b]*Novosibirsk State University, Novosibirsk 630090, Russia*
[8c]*Novosibirsk State Technical University, Novosibirsk 630092, Russia*
[9]*University of California at Irvine, Irvine, California 92697, USA*
[10]*University of California at Riverside, Riverside, California 92521, USA*
[11]*University of California at Santa Cruz, Institute for Particle Physics, Santa Cruz, California 95064, USA*
[12]*California Institute of Technology, Pasadena, California 91125, USA*
[13]*University of Cincinnati, Cincinnati, Ohio 45221, USA*

[14]University of Colorado, Boulder, Colorado 80309, USA
[15]Laboratoire Leprince-Ringuet, Ecole Polytechnique, CNRS/IN2P3, F-91128 Palaiseau, France
[16a]INFN Sezione di Ferrara, I-44122 Ferrara, Italy
[16b]Dipartimento di Fisica e Scienze della Terra, Università di Ferrara, I-44122 Ferrara, Italy
[17]INFN Laboratori Nazionali di Frascati, I-00044 Frascati, Italy
[18]INFN Sezione di Genova, I-16146 Genova, Italy
[19]Humboldt-Universität zu Berlin, Institut für Physik, D-12489 Berlin, Germany
[20]Indian Institute of Technology Guwahati, Guwahati 781 039, Assam, India
[21]University of Iowa, Iowa City, Iowa 52242, USA
[22]Iowa State University, Ames, Iowa 50011, USA
[23]Johns Hopkins University, Baltimore, Maryland 21218, USA
[24]Laboratoire de l'Accélérateur Linéaire, IN2P3/CNRS et Université Paris-Sud 11, Centre Scientifique d'Orsay, F-91898 Orsay Cedex, France
[25]Lawrence Livermore National Laboratory, Livermore, California 94550, USA
[26]University of Liverpool, Liverpool L69 7ZE, United Kingdom
[27]Queen Mary, University of London, London E1 4NS, United Kingdom
[28]University of London, Royal Holloway and Bedford New College, Egham, Surrey TW20 0EX, United Kingdom
[29]University of Louisville, Louisville, Kentucky 40292, USA
[30]Johannes Gutenberg-Universität Mainz, Institut für Kernphysik, D-55099 Mainz, Germany
[31]University of Manchester, Manchester M13 9PL, United Kingdom
[32]University of Maryland, College Park, Maryland 20742, USA
[33]Massachusetts Institute of Technology, Laboratory for Nuclear Science, Cambridge, Massachusetts 02139, USA
[34a]Institute of Particle Physics, Montréal, Québec H3A 2T8, Canada
[34b]McGill University, Montréal, Québec H3A 2T8, Canada
[35a]INFN Sezione di Milano, I-20133 Milano, Italy
[35b]Dipartimento di Fisica, Università di Milano, I-20133 Milano, Italy
[36]University of Mississippi, University, Mississippi 38677, USA
[37]Université de Montréal, Physique des Particules, Montréal, Québec H3C 3J7, Canada
[38]INFN Sezione di Napoli and Dipartimento di Scienze Fisiche, Università di Napoli Federico II, I-80126 Napoli, Italy
[39]NIKHEF, National Institute for Nuclear Physics and High Energy Physics, NL-1009 DB Amsterdam, Netherlands
[40]University of Notre Dame, Notre Dame, Indiana 46556, USA
[41]Ohio State University, Columbus, Ohio 43210, USA
[42a]INFN Sezione di Padova, I-35131 Padova, Italy
[42b]Dipartimento di Fisica, Università di Padova, I-35131 Padova, Italy
[43]Laboratoire de Physique Nucléaire et de Hautes Energies, IN2P3/CNRS, Université Pierre et Marie Curie-Paris6, Université Denis Diderot-Paris7, F-75252 Paris, France
[44a]INFN Sezione di Perugia, I-06123 Perugia, Italy
[44b]Dipartimento di Fisica, Università di Perugia, I-06123 Perugia, Italy
[45a]INFN Sezione di Pisa, I-56127 Pisa, Italy
[45b]Dipartimento di Fisica, Università di Pisa, I-56127 Pisa, Italy
[45c]Scuola Normale Superiore di Pisa, I-56127 Pisa, Italy
[46]Princeton University, Princeton, New Jersey 08544, USA
[47a]INFN Sezione di Roma, I-00185 Roma, Italy
[47b]Dipartimento di Fisica, Università di Roma La Sapienza, I-00185 Roma, Italy
[48]Universität Rostock, D-18051 Rostock, Germany
[49]Rutherford Appleton Laboratory, Chilton, Didcot, Oxon OX11 0QX, United Kingdom
[50]CEA, Irfu, SPP, Centre de Saclay, F-91191 Gif-sur-Yvette, France
[51]SLAC National Accelerator Laboratory, Stanford, California 94309, USA
[52]University of South Carolina, Columbia, South Carolina 29208, USA
[53]Southern Methodist University, Dallas, Texas 75275, USA
[54]St. Francis Xavier University, Antigonish, Nova Scotia B2G 2W5, Canada
[55]Stanford University, Stanford, California 94305, USA
[56]State University of New York, Albany, New York 12222, USA
[57]Tel Aviv University, School of Physics and Astronomy, Tel Aviv 69978, Israel
[58]University of Tennessee, Knoxville, Tennessee 37996, USA
[59]University of Texas at Austin, Austin, Texas 78712, USA

[60]University of Texas at Dallas, Richardson, Texas 75083, USA
[61a]INFN Sezione di Torino, I-10125 Torino, Italy
[61b]Dipartimento di Fisica, Università di Torino, I-10125 Torino, Italy
[62]INFN Sezione di Trieste and Dipartimento di Fisica, Università di Trieste, I-34127 Trieste, Italy
[63]IFIC, Universitat de Valencia-CSIC, E-46071 Valencia, Spain
[64a]Institute of Particle Physics, Victoria, British Columbia V8W 3P6, Canada
[64b]University of Victoria, Victoria, British Columbia V8W 3P6, Canada
[65]Department of Physics, University of Warwick, Coventry CV4 7AL, United Kingdom
[66]University of Wisconsin, Madison, Wisconsin 53706, USA

(Received 12 April 2018; published 21 June 2018)

We study the $\Upsilon(1S)$ radiative decays to $\gamma\pi^+\pi^-$ and γK^+K^- using data recorded with the *BABAR* detector operating at the SLAC PEP-II asymmetric-energy e^+e^- collider at center-of-mass energies at the $\Upsilon(2S)$ and $\Upsilon(3S)$ resonances. The $\Upsilon(1S)$ resonance is reconstructed from the decay $\Upsilon(nS)\to\pi^+\pi^-\Upsilon(1S)$, $n=2,3$. Branching fraction measurements and spin-parity analyses of $\Upsilon(1S)$ radiative decays are reported for the $I=0$ S-wave and $f_2(1270)$ resonances in the $\pi^+\pi^-$ mass spectrum, the $f_2'(1525)$ and $f_0(1500)$ in the K^+K^- mass spectrum, and the $f_0(1710)$ in both.

DOI: 10.1103/PhysRevD.97.112006

I. INTRODUCTION

The existence of gluonium states is still an open issue for quantum chromodynamics (QCD). Lattice QCD calculations predict the lightest gluonium states to have quantum numbers $J^{PC}=0^{++}$ and 2^{++} and to be in the mass region below 2.5 GeV/c^2 [1]. In particular, the $J^{PC}=0^{++}$ glueball is predicted to have a mass around 1.7 GeV/c^2. Searches for these states have been performed using many supposed "gluon rich" reactions. However, despite intense experimental searches, there is no conclusive experimental evidence for their direct observation [2,3]. The identification of the scalar glueball is further complicated by the possible mixing with standard $q\bar{q}$ states. The broad $f_0(500)$, $f_0(1370)$ [4], $f_0(1500)$ [5,6], and $f_0(1710)$ [7] have been suggested as scalar glueball candidates. A feature of the scalar glueball is that its $s\bar{s}$ decay mode should be favored with respect to $u\bar{u}$ or $d\bar{d}$ decay modes [8,9].

Radiative decays of heavy quarkonia, in which a photon replaces one of the three gluons from the strong decay of J/ψ or $\Upsilon(1S)$, can probe color-singlet two-gluon systems that produce gluonic resonances. Recently, detailed calculations have been performed on the production rates of the scalar glueball in the process $V(1^{--})\to\gamma G$, where G indicates the scalar glueball and $V(1^{--})$ indicates charmonium or bottomonium vector mesons such as J/ψ, $\psi(2S)$, or $\Upsilon(1S)$ [10–13].

J/ψ decays have been extensively studied in the past [14] and are currently analyzed in e^+e^- interactions by BES experiments [15,16]. The experimental observation of radiative $\Upsilon(1S)$ decays is challenging because their rate is suppressed by a factor of $\approx$0.025 compared to J/ψ radiative decays, which are of order 10^{-3} [17]. Radiative $\Upsilon(1S)$ decays to a pair of hadrons have been studied by the CLEO Collaboration [17,18] with limited statistics and large backgrounds from $e^+e^-\to\gamma$ (vector meson). In this work, we observe $\Upsilon(1S)$ decays through the decay chain $\Upsilon(2S)/\Upsilon(3S)\to\pi^+\pi^-\Upsilon(1S)$. This allows us to study $\Upsilon(1S)$ radiative decays to $\pi^+\pi^-$ and K^+K^- final states with comparable statistics, but lower background.

This paper is organized as follows. In Sec. II, we give a brief description of the *BABAR* detector, and Sec. III is devoted to the description of event reconstruction. In Sec. IV, we study resonance production in $\pi^+\pi^-$ and K^+K^- final states, and Sec. V is devoted to the description of the efficiency correction. We describe in Sec. VI a study of the angular distributions using a Legendre polynomial moments analysis, while Sec. VII gives results on the full angular analysis. The measurement of the branching fractions is described in Sec. VIII, and the results are summarized in Sec. IX.

II. THE *BABAR* DETECTOR AND DATA SET

The results presented here are based on data collected by the *BABAR* detector with the PEP-II asymmetric-energy

[*]Deceased
[†]Present address: Wuhan University, Wuhan 430072, China.
[‡]Present address: Università di Bologna and INFN Sezione di Bologna, I-47921 Rimini, Italy.
[§]Present address: University of Huddersfield, Huddersfield HD1 3DH, United Kingdom.
[‖]Present address: University of South Alabama, Mobile, Alabama 36688, USA.
[¶]Also at Università di Sassari, I-07100 Sassari, Italy.

e^+e^- collider located at SLAC, at the $\Upsilon(2S)$ and $\Upsilon(3S)$ resonances with integrated luminosities [19] of 13.6 and 28.0 fb^{-1}, respectively. The *BABAR* detector is described in detail elsewhere [20]. The momenta of charged particles are measured by means of a five-layer, double-sided microstrip detector, and a 40-layer drift chamber, both operating in the 1.5 T magnetic field of a superconducting solenoid. Photons are measured and electrons are identified in a CsI(Tl) crystal electromagnetic calorimeter (EMC). Charged-particle identification is provided by the measurement of specific energy loss in the tracking devices, and by an internally reflecting, ring-imaging Cherenkov detector. Muons and K^0_L mesons are detected in the instrumented flux return of the magnet. Monte Carlo (MC) simulated events [21], with reconstructed sample sizes more than 100 times larger than the corresponding data samples, are used to evaluate the signal efficiency.

III. EVENTS RECONSTRUCTION

We reconstruct the decay chains

$$\Upsilon(2S)/\Upsilon(3S) \to (\pi^+_s\pi^-_s)\Upsilon(1S) \to (\pi^+_s\pi^-_s)(\gamma\pi^+\pi^-) \quad (1)$$

and

$$\Upsilon(2S)/\Upsilon(3S) \to (\pi^+_s\pi^-_s)\Upsilon(1S) \to (\pi^+_s\pi^-_s)(\gamma K^+K^-), \quad (2)$$

where we label with the subscript s the slow pions from the direct $\Upsilon(2S)$ and $\Upsilon(3S)$ decays. We consider only events containing exactly four well-measured tracks with transverse momentum greater than 0.1 GeV/c and a total net charge equal to zero. We also require exactly one well-reconstructed γ in the EMC having an energy greater than 2.5 GeV. To remove background originating from π^0 mesons we remove events having π^0 candidates formed with photons having an energy greater than 100 MeV. The four tracks are fitted to a common vertex, with the requirements that the fitted vertex be within the e^+e^- interaction region and have a χ^2 fit probability greater than 0.001. We select muons, electrons, kaons, and pions by applying high-efficiency particle identification criteria [22]. For each track we test the electron and muon identification hypotheses and remove the event if any of the charged tracks satisfies a tight muon or electron identification criterion.

We require momentum balance for the four final states, making use of a χ^2 distribution defined as

$$\chi^2 = \sum_{i=1}^{3} \frac{(\Delta\mathbf{p}_i - \langle\Delta\mathbf{p}_i\rangle)^2}{\sigma_i^2}, \quad (3)$$

where $\Delta\mathbf{p}_i$ are the missing laboratory three-momenta components

$$\Delta\mathbf{p}_i = \mathbf{p}_i^{e^+} + \mathbf{p}_i^{e^-} - \sum_{j=1}^{5}\mathbf{p}_i^j, \quad (4)$$

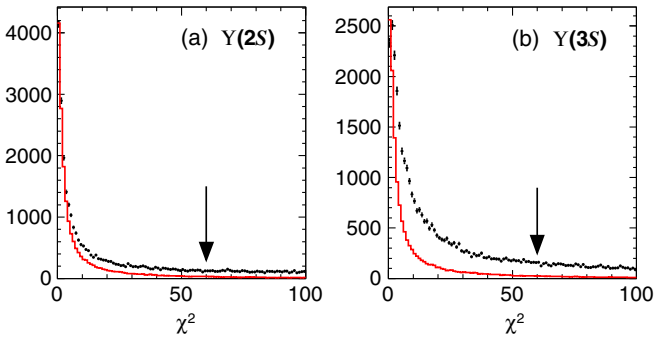

FIG. 1. χ^2 distributions used for defining the momentum balance for data (black dots) compared with signal MC simulations (full (red) line) for (a) $\Upsilon(2S)$ and (b) $\Upsilon(3S)$ data from reactions (1). The arrows indicate the cutoff used to select momentum balancing events.

and $\langle\Delta\mathbf{p}_i\rangle$ and σ_i are the mean values and the widths of the missing momentum distributions. These are obtained from signal MC simulations of the four final states through two or three Gaussian function fits to the MC balanced momentum distributions. When multiple Gaussian functions are used, the mean values and σ quoted are average values weighted by the relative fractions. In Eq. (4), $\mathbf{p}_i$ indicates the three components of the laboratory momenta of the five particles in the final state, while $\mathbf{p}_i^{e^+}$ and $\mathbf{p}_i^{e^-}$ indicate the three-momenta of the incident beams.

Figure 1 shows the χ^2 distributions for reactions (a) $\Upsilon(2S) \to (\pi^+_s\pi^-_s)\Upsilon(1S) \to (\pi^+_s\pi^-_s)(\gamma\pi^+\pi^-)$ and (b) $\Upsilon(3S) \to (\pi^+_s\pi^-_s)\Upsilon(1S) \to (\pi^+_s\pi^-_s)(\gamma\pi^+\pi^-)$, respectively compared with signal MC simulations. The accumulations at thresholds represent events satisfying momentum balance. We apply a very loose selection, $\chi^2 < 60$, optimized using the $\Upsilon(2S)$ data, and remove events consistent with being entirely due to background. We note a higher background in the $\Upsilon(3S)$ data, but keep the same loose selection to achieve a similar efficiency.

Events with balanced momentum are then required to satisfy energy balance requirements. In the above decays, the π_s originating from direct $\Upsilon(2S)/\Upsilon(3S)$ decays have a soft laboratory momentum distribution (< 600 MeV/c), partially overlapping with the hard momentum distributions for the hadrons originating from the $\Upsilon(1S)$ decay. We therefore require energy balance, following a combinatorial approach.

For each combination of $\pi^+_s\pi^-_s$ candidates, we first require both particles to be identified loosely as pions and compute the recoiling mass,

$$M^2_{\rm rec}(\pi^+_s\pi^-_s) = |p_{e^+} + p_{e^-} - p_{\pi^+_s} - p_{\pi^-_s}|^2, \quad (5)$$

where p is the particle four-momentum. The distribution of $M^2_{\rm rec}(\pi^+_s\pi^-_s)$ is expected to peak at the squared $\Upsilon(1S)$ mass for signal events. Figure 2 shows the combinatorial

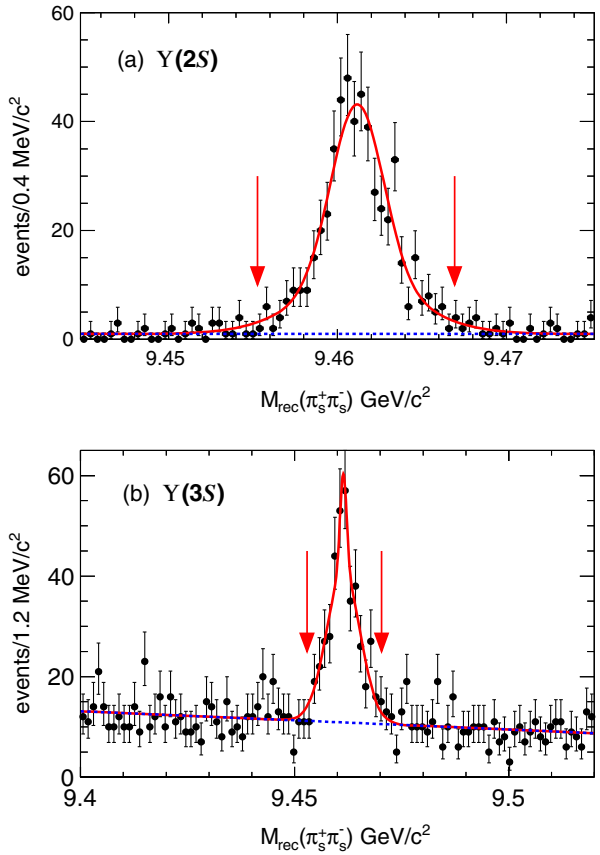

FIG. 2. Combinatorial recoiling mass $M_{\rm rec}$ to $\pi_s^+\pi_s^-$ candidates for (a) $\Upsilon(2S)$ and (b) $\Upsilon(3S)$ data. The lines are the results from the fit described in the text. The arrows indicate the selections used to apply the energy balance criterion.

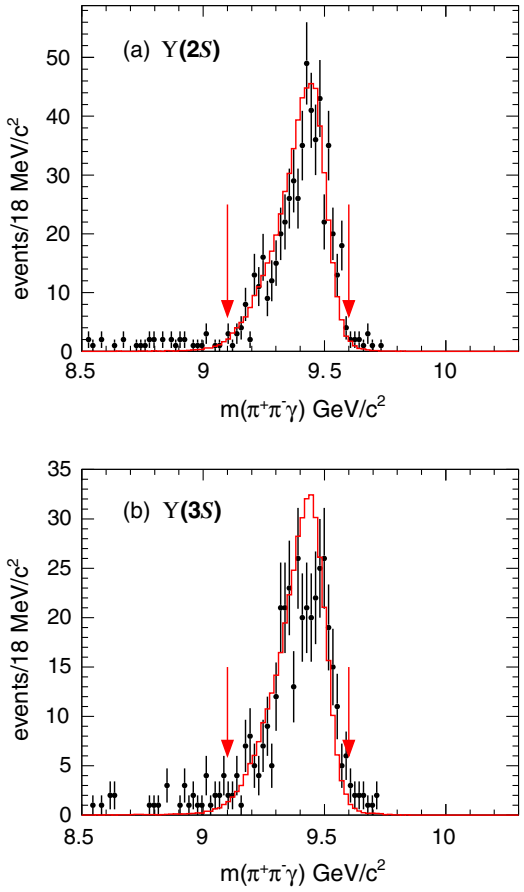

FIG. 3. $m(\gamma\pi^+\pi^-)$ mass distributions after the $M_{\rm rec}(\pi_s^+\pi_s^-)$ selection for the (a) $\Upsilon(2S)$ and (b) $\Upsilon(3S)$ data. The arrows indicate the range used to select the $\Upsilon(1S)$ signal. The full line histograms are the results from signal MC simulations.

recoiling mass $M_{\rm rec}(\pi_s^+\pi_s^-)$ for $\Upsilon(2S)$ and $\Upsilon(3S)$ data, where narrow peaks at the $\Upsilon(1S)$ mass can be observed.

We fit each of these distributions using a linear function for the background and the sum of two Gaussian functions for the signal, obtaining average $\sigma = 2.3$ MeV/c^2 and $\sigma = 3.5$ MeV/c^2 values for the $\Upsilon(2S)$ and $\Upsilon(3S)$ data, respectively. We select signal event candidates by requiring

$$|M_{\rm rec}(\pi_s^+\pi_s^-) - m(\Upsilon(1S))_f| < 2.5\sigma, \tag{6}$$

where $m(\Upsilon(1S))_f$ indicates the fitted $\Upsilon(1S)$ mass value. We obtain, in the above mass window, values of signal-to-background ratios of 517/40 and 276/150 for $\Upsilon(2S)$ and $\Upsilon(3S)$ data, respectively.

To reconstruct $\Upsilon(1S) \to \gamma\pi^+\pi^-$ decays, we require a loose identification of both pions from the $\Upsilon(1S)$ decay and obtain the distributions of $m(\gamma\pi^+\pi^-)$ shown in Fig. 3. The distributions show the expected peak at the $\Upsilon(1S)$ mass with little background but do not have a Gaussian shape due to the asymmetric energy response of the EMC to a high-energy photon. The full line histograms compare the data with signal MC simulations and show good agreement.

We finally isolate the decay $\Upsilon(1S) \to \gamma\pi^+\pi^-$ by requiring

$$9.1\ {\rm GeV}/c^2 < m(\gamma\pi^+\pi^-) < 9.6\ {\rm GeV}/c^2. \tag{7}$$

At this stage no more than one candidate per event is present.

We reconstruct the final state where $\Upsilon(1S) \to \gamma K^+K^-$ in a similar manner, by applying a loose identification of both kaons in the final state and requiring the $m(K^+K^-\gamma)$ mass, shown in Fig. 4, to be in the range

$$9.1\ {\rm GeV}/c^2 < m(K^+K^-\gamma) < 9.6\ {\rm GeV}/c^2. \tag{8}$$

IV. STUDY OF THE $\pi^+\pi^-$ AND K^+K^- MASS SPECTRA

The $\pi^+\pi^-$ mass spectrum, for $m(\pi^+\pi^-) < 3.0$ GeV/c^2 and summed over the $\Upsilon(2S)$ and $\Upsilon(3S)$ data sets with 507 and 277 events, respectively, is shown in Fig. 5(a). The resulting K^+K^- mass spectrum, summed over the $\Upsilon(2S)$

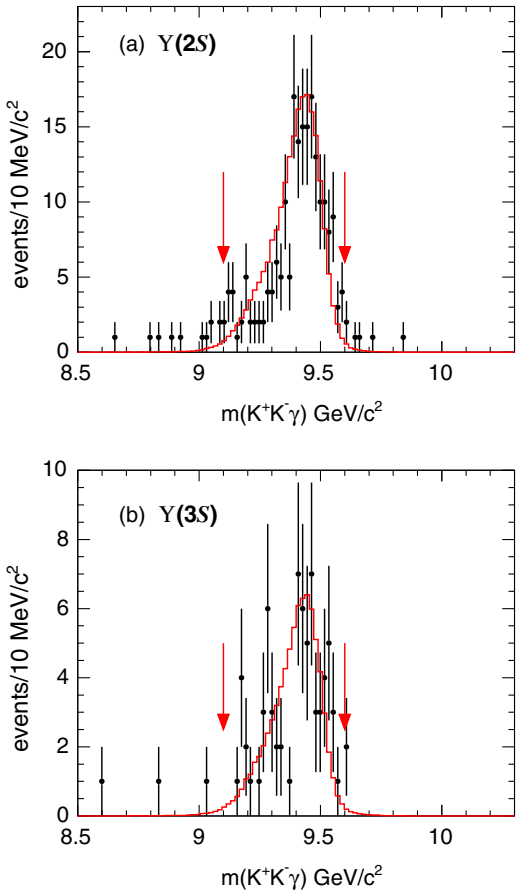

FIG. 4. $m(K^+K^-\gamma)$ mass distributions after the $M_{\rm rec}(\pi_s^+\pi_s^-)$ selection for the (a) $\Upsilon(2S)$ and (b) $\Upsilon(3S)$ data. The arrows indicate the range used to select the $\Upsilon(1S)$ signal. The full line histograms are the results from signal MC simulations.

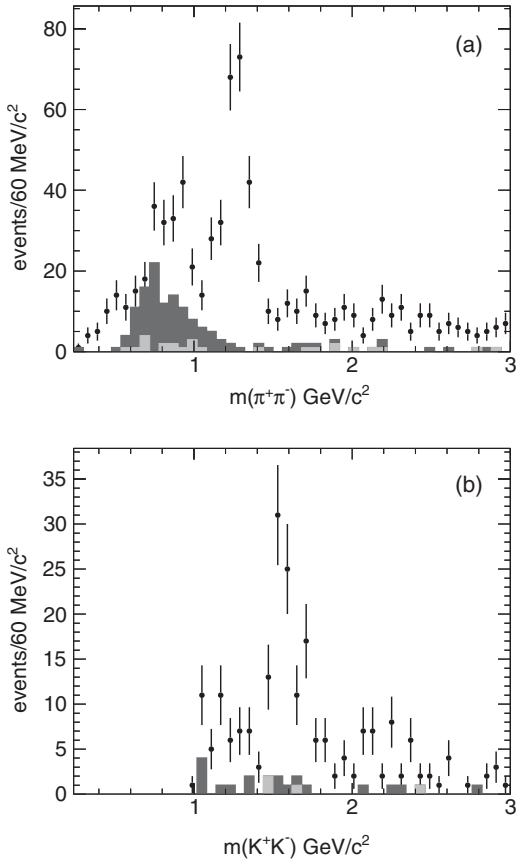

FIG. 5. (a) $\pi^+\pi^-$ mass distribution from $\Upsilon(1S) \to \pi^+\pi^-\gamma$ for the combined $\Upsilon(2S)$ and $\Upsilon(3S)$ data sets. (b) K^+K^- mass distribution from $\Upsilon(1S) \to K^+K^-\gamma$ for the combined $\Upsilon(2S)$ and $\Upsilon(3S)$ data sets. The gray distributions show the expected background obtained from the corresponding $M_{\rm rec}(\pi_s^+\pi_s^-)$ sidebands. The light-gray distributions evidences the background contribution from the $\Upsilon(2S)$ data.

and $\Upsilon(3S)$ data sets with 164 and 63 events, respectively, is shown in Fig. 5(b). For a better comparison the two distributions are plotted using the same bin size and the same mass range.

We study the background for both $\pi^+\pi^-$ and K^+K^- final states using the $M_{\rm rec}(\pi_s^+\pi_s^-)$ sidebands. We select events in the $(4.5\sigma - 7.0\sigma)$ regions on both sides of the signal region and require the $m(\pi^+\pi^-\gamma)$ and $m(K^+K^-\gamma)$ to be in the ranges defined by Eqs. (7) and (8), respectively. The resulting $\pi^+\pi^-$ and K^+K^- mass spectra for these events are superimposed in gray in Figs. 5(a) and 5(b), respectively. We note rather low background levels for all the final states, except for the $\pi^+\pi^-$ mass spectrum from the $\Upsilon(3S)$ data, which shows an enhancement at a mass of $\approx$750 MeV/c^2, which we attribute to the presence of $\rho(770)^0$ background. The $\pi^+\pi^-$ mass spectrum from inclusive $\Upsilon(3S)$ decays also shows a strong $\rho(770)^0$ contribution.

We search for background originating from a possible hadronic $\Upsilon(1S) \to \pi^+\pi^-\pi^0$ decay, where one of the two γ's from the π^0 decay is lost. For this purpose, we make use of the $\Upsilon(2S)$ data and select events having four charged pions and only one π^0 candidate. We then select events satisfying Eq. (6) and plot the $\pi^+\pi^-\pi^0$ effective mass distribution. No $\Upsilon(1S)$ signal is observed, which indicates that the branching fraction for this possible $\Upsilon(1S)$ decay mode is very small and therefore that no contamination is expected in the study of the $\Upsilon(1S) \to \gamma\pi^+\pi^-$ decay mode.

The $\pi^+\pi^-$ mass spectrum, in 30 MeV/c^2 bin size is shown in Fig. 6. The spectrum shows $I = 0$, $J^P = \text{even}^{++}$ resonance production, with low backgrounds above 1 GeV/c^2. We observe a rapid drop around 1 GeV/c^2 characteristic of the presence of the $f_0(980)$, and a strong $f_2(1270)$ signal. The data also suggest the presence of weaker resonant contributions. The K^+K^- mass spectrum is shown in Fig. 7 and also shows resonant production, with low background. Signals at the positions of $f_2'(1525)$ and $f_0(1710)$ can be observed.

We make use of a phenomenological model to extract the different $\Upsilon(1S) \to \gamma R$ branching fractions, where R is an intermediate resonance.

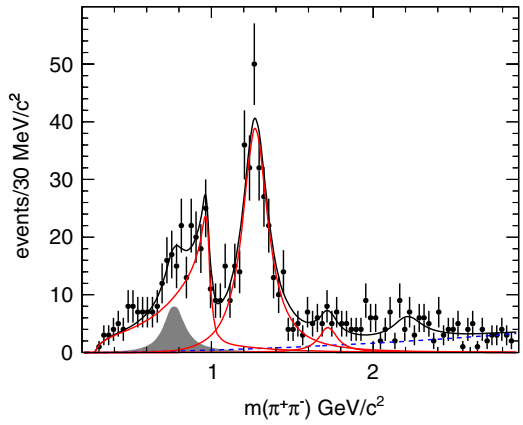

FIG. 6. $\pi^+\pi^-$ mass distribution from $\Upsilon(1S) \to \pi^+\pi^-\gamma$ for the combined $\Upsilon(2S)$ and $\Upsilon(3S)$ data sets. The full (black) line is the results from the fit, the dashed (blue) line represents the fitted background. The full (red) curves indicate the S-wave, $f_2(1270)$, and $f_0(1710)$ contributions. The shaded (gray) area represents the fitted $\rho(770)^0$ background.

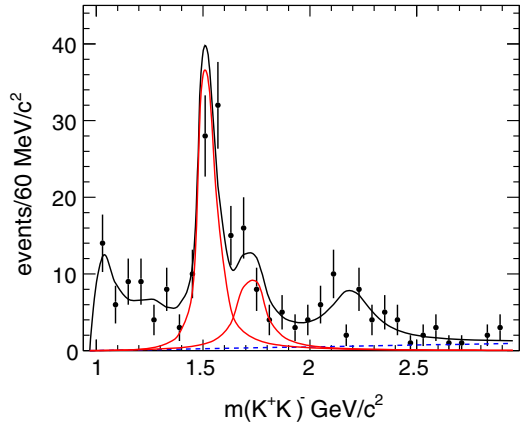

FIG. 7. K^+K^- mass distribution from $\Upsilon(1S) \to K^+K^-\gamma$ for the combined $\Upsilon(2S)$ and $\Upsilon(3S)$ data sets. The full (black) line is the results from the fit, the dashed (blue) line represents the fitted background. The (red) curves show the contributions from $f_2'(1525)$ and $f_0(1710)$.

A. Fit to the $\pi^+\pi^-$ mass spectrum

We perform a simultaneous binned fit to the $\pi^+\pi^-$ mass spectra from the $\Upsilon(2S)$ and $\Upsilon(3S)$ data sets using the following model.

(i) We describe the low-mass region (around the $f_0(500)$) using a relativistic S-wave Breit-Wigner lineshape having free parameters. We test the S-wave hypothesis in Secs. VI and VIII. We obtain its parameters from the $\Upsilon(2S)$ data only, and we fix them in the description of the $\Upsilon(3S)$ data.

(ii) We describe the $f_0(980)$ using the Flatté [23] formalism. For the $\pi^+\pi^-$ channel the Breit-Wigner lineshape has the form

$$\mathrm{BW}(m) = \frac{m_0\sqrt{\Gamma_i}\sqrt{\Gamma_\pi(m)}}{m_0^2 - m^2 - im_0(\Gamma_\pi(m) + \Gamma_K(m))}, \quad (9)$$

and in the K^+K^- channel the Breit-Wigner function has the form

$$\mathrm{BW}(m) = \frac{m_0\sqrt{\Gamma_i}\sqrt{\Gamma_K(m)}}{m_0^2 - m^2 - im_0(\Gamma_\pi(m) + \Gamma_K(m))}, \quad (10)$$

where Γ_i is absorbed into the intensity of the resonance. $\Gamma_\pi(m)$ and $\Gamma_K(m)$ describe the partial widths of the resonance to decay to $\pi\bar{\pi}$ and $K\bar{K}$ and are given by

$$\Gamma_\pi(m) = g_\pi\left(\frac{m^2}{4} - m_\pi^2\right)^{1/2},$$
$$\Gamma_K(m) = \frac{g_K}{2}\left[\left(\frac{m^2}{4} - m_{K^+}^2\right)^{1/2} + \left(\frac{m^2}{4} - m_{K^0}^2\right)^{1/2}\right], \quad (11)$$

where g_π and g_K are the squares of the coupling constants of the resonance to the $\pi\bar{\pi}$ and $K\bar{K}$ systems. The $f_0(980)$ parameters and couplings are taken from Ref. [24]: $m_0 = 0.979 \pm 0.004$ GeV/c^2, $g_\pi = 0.28 \pm 0.04$ and $g_K = 0.56 \pm 0.18$.

(iii) The total S-wave is described by a coherent sum of $f_0(500)$ and $f_0(980)$ as

$$S\text{-wave} = |\mathrm{BW}_{f_0(500)}(m) + c\mathrm{BW}_{f_0(980)}(m)e^{i\phi}|^2. \quad (12)$$

where c and ϕ are free parameters for the relative intensity and phase of the two interfering contributions.

(iv) The $f_2(1270)$ and $f_0(1710)$ resonances are represented by relativistic Breit-Wigner functions with parameters fixed to PDG values [25].

(v) In the high $\pi^+\pi^-$ mass region, we are unable, with the present statistics, to distinguish the different possible resonant contributions. Therefore we make use of the method used by CLEO [26] and include a single resonance $f_0(2100)$ having a width fixed to the PDG value (224 ± 22) and unconstrained mass.

(vi) The background is parametrized with a quadratic dependence

$$b(m) = p(m)(a_1 m + a_2 m^2),$$

where $p(m)$ is the π center-of-mass momentum in the $\pi^+\pi^-$ rest frame, which goes to zero at $\pi^+\pi^-$ threshold.

(vii) For the $\Upsilon(3S)$ data we also include $\rho(770)^0$ background with parameters fixed to the PDG values.

TABLE I. Resonances yields and statistical significances from the fits to the $\pi^+\pi^-$ and K^+K^- mass spectra for the $\Upsilon(2S)$ and $\Upsilon(3S)$ data sets. The symbol $f_J(1500)$ indicates the signal in the 1500 MeV/c^2 mass region. When two errors are reported, the first is statistical and the second systematic. Systematic uncertainties are evaluated only for resonances for which we compute branching fractions.

Resonances ($\pi^+\pi^-$)	Yield $\Upsilon(2S)$	Yield $\Upsilon(3S)$	Significance
S-wave	$133 \pm 16 \pm 13$	87 ± 13	12.8σ
$f_2(1270)$	$255 \pm 19 \pm 8$	$77 \pm 7 \pm 4$	15.9σ
$f_0(1710)$	$24 \pm 8 \pm 6$	$6 \pm 8 \pm 3$	2.5σ
$f_0(2100)$	33 ± 9	8 ± 15	
$\rho(770)^0$		54 ± 23	
Resonances (K^+K^-)	Yield $\Upsilon(2S) + \Upsilon(3S)$		Significance
$f_0(980)$	47 ± 9		5.6σ
$f_J(1500)$	$77 \pm 10 \pm 10$		8.9σ
$f_0(1710)$	$36 \pm 9 \pm 6$		4.7σ
$f_2(1270)$	15 ± 8		
$f_0(2200)$	38 ± 8		

The fit is shown in Fig. 6. It has 16 free parameters and $\chi^2 = 182$ for ndf $= 152$, corresponding to a p-value of 5%. The yields and statistical significances are reported in Table I. Significances are computed as follows: for each resonant contribution (with fixed parameters) we set the yield to zero and compute the significance as $\sigma = \sqrt{\Delta\chi^2}$, where $\Delta\chi^2$ is the difference in χ^2 between the fit with and without the presence of the resonance.

The table also reports systematic uncertainties on the yields, evaluated as follows: the parameters of each resonance are modified according to $\pm\sigma$, where σ is the PDG uncertainty and the deviations from the reference fit are added in quadrature. The background has been modified to have a linear shape. The effective range in the Blatt-Weisskopf [27] factors entering in the description of the intensity and the width of the relativistic Breit-Wigner function have been varied between 1 and 5 GeV^{-1}, and the average deviation is taken as a systematic uncertainty. The different contributions, dominated by the uncertainties on the resonances parameters, are added in quadrature.

We note the observation of a significant S-wave in $\Upsilon(1S)$ radiative decays. This observation was not possible in the study of J/ψ radiative decay to $\pi^+\pi^-$ because of the presence of a strong, irreducible background from $J/\psi \to \pi^+\pi^-\pi^0$ [28]. We obtain the following $f_0(500)$ parameters:

$$m(f_0(500)) = 0.856 \pm 0.086 \text{ GeV}/c^2,$$
$$\Gamma(f_0(500)) = 1.279 \pm 0.324 \text{ GeV}, \quad (13)$$

and $\phi = 2.41 \pm 0.43$ rad. The fraction of S-wave events associated with the $f_0(500)$ is $(27.7 \pm 3.1)\%$. We also obtain $m(f_0(2100)) = 2.208 \pm 0.068$ GeV/c^2.

B. Study of the K^+K^- mass spectrum

Due to the limited statistics we do not separate the data into the $\Upsilon(2S)$ and $\Upsilon(3S)$ data sets. We perform a binned fit to the combined K^+K^- mass spectrum using the following model:

(i) The background is parametrized with a linear dependence starting with zero at threshold.
(ii) The $f_0(980)$ is parametrized according to the Flatté formalism described by Eq. (10) for the K^+K^- projection.
(iii) The $f_2(1270)$, $f_2'(1525)$, $f_0(1500)$, and $f_0(1710)$ resonances are represented by relativistic Breit-Wigner functions with parameters fixed to PDG values.
(iv) We include an $f_0(2200)$ contribution having parameters fixed to the PDG values.

The fit shown in Fig. 7. It has six free parameters and $\chi^2 = 35$ for ndf $= 29$, corresponding to a p-value of 20%; the yields and significances are reported in Table I. Systematic uncertainties have been evaluated as for the fit to the $\pi^+\pi^-$ mass spectrum. The parameters of each resonance are modified according to $\pm\sigma$, where σ is the PDG uncertainty and the deviations from the reference fit are added in quadrature. The background has been modified to have a quadratic shape. The effective range in the Blatt-Weisskopf [27] factors entering in the description of the intensity and the width of the relativistic Breit-Wigner function have been varied between 1 and 5 GeV^{-1}, and the average deviation is taken as a systematic uncertainty. The different contributions, dominated by the uncertainties on the resonances parameters, are added in quadrature. In the 1500 MeV/c^2 mass region, both $f_2'(1525)$ and $f_0(1500)$ can contribute, therefore we first fit the mass spectrum assuming the presence of $f_2'(1525)$ only and then replace in the fit the $f_2'(1525)$ with the $f_0(1500)$ resonance. In Table I, we label this contribution as $f_J(1500)$. The resulting yield variation between the two fits is small and gives a negligible contribution to the total systematic uncertainty. A separation of the $f_2'(1525)$ and $f_0(1500)$ contributions is discussed in Secs. VI and VII.

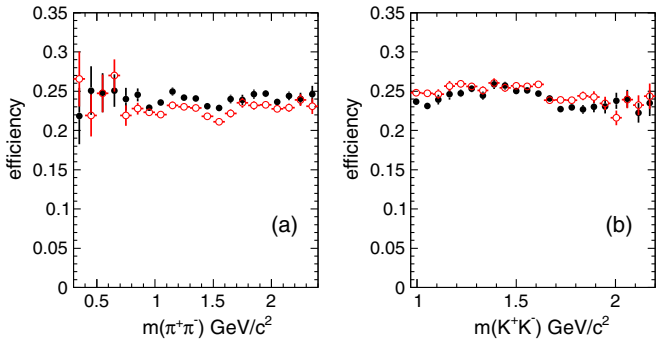

FIG. 8. Efficiency distributions as function of mass for the $\Upsilon(2S)/\Upsilon(3S)$ data. (a) $\pi^+\pi^-\gamma$, (b) $K^+K^-\gamma$. Filled (black) circles are for $\Upsilon(2S)$ data, open (red) circles are for $\Upsilon(3S)$ data.

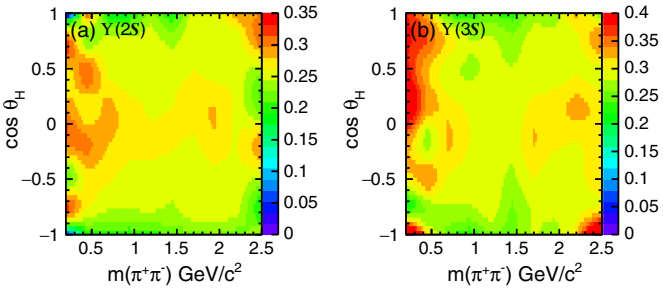

FIG. 9. Fitted efficiency distribution in the $(m(\pi^+\pi^-), \cos\theta_H)$ plane for $\Upsilon(1S) \to \gamma\pi^+\pi^-$ for the (a) $\Upsilon(2S)$ and (b) $\Upsilon(3S)$ data sets.

V. EFFICIENCY CORRECTION

A. Reconstruction efficiency

To compute the efficiency, MC signal events are generated using a detailed detector simulation [21]. These simulated events are reconstructed and analyzed in the same manner as data. The efficiency is computed as the ratio between reconstructed and generated events. The efficiency distributions as functions of mass, for the $\Upsilon(2S)/\Upsilon(3S)$ data and for the $\pi^+\pi^-\gamma$ and $K^+K^-\gamma$ final states, are shown in Fig. 8. We observe an almost uniform behavior for all the final states.

We define the helicity angle θ_H as the angle formed by the h^+ (where $h = \pi, K$), in the h^+h^- rest frame, and the γ in the $h^+h^-\gamma$ rest frame. We also define θ_γ as the angle formed by the radiative photon in the $h^+h^-\gamma$ rest frame with respect to the $\Upsilon(1S)$ direction in the $\Upsilon(2S)/\Upsilon(3S)$ rest frame.

We compute the efficiency in two different ways.

(i) We label with $\epsilon(m, \cos\theta_H)$ the efficiency computed as a function of the h^+h^- effective mass and the helicity angle $\cos\theta_H$. This is used only to obtain efficiency-corrected mass spectra.

(ii) We label with $\epsilon(\cos\theta_H, \cos\theta_\gamma)$ the efficiency computed, for each resonance mass window (defined in Table III), as a function of $\cos\theta_H$ and $\cos\theta_\gamma$. This is used to obtain the efficiency-corrected angular distributions and branching fractions of the different resonances.

To smoothen statistical fluctuations in the evaluation of $\epsilon(m, \cos\theta_H)$, for $\Upsilon(1S) \to \gamma\pi^+\pi^-$, we divide the $\pi^+\pi^-$ mass into nine 300-MeV/c^2-wide intervals and plot the $\cos\theta_H$ in each interval. The distributions of $\cos\theta_H$ are then fitted using cubic splines [29]. The efficiency at each $m(\pi^+\pi^-)$ is then computed using a linear interpolation between adjacent bins.

Figure 9 shows the efficiency distributions in the $(m(\pi^+\pi^-), \cos\theta_H)$ plane for the $\Upsilon(2S)$ and $\Upsilon(3S)$ data sets. We observe an almost uniform behavior with some loss at $\cos\theta_H$ close to ± 1. The efficiencies integrated over $\cos\theta_H$ are consistent with being constant with mass and have average values of $\epsilon(\Upsilon(2S) \to \pi^+\pi^-\Upsilon(1S)(\to \gamma\pi^+\pi^-)) = 0.237 \pm 0.001$ and $\epsilon(\Upsilon(3S) \to \pi^+\pi^-\Upsilon(1S)(\to \gamma\pi^+\pi^-)) = 0.261 \pm 0.001$.

A similar method is used to compute $\epsilon(m, \cos\theta_H)$ for the $\Upsilon(1S) \to \gamma K^+K^-$ final state. The average efficiency values are $\epsilon(\Upsilon(2S) \to \pi^+\pi^-\Upsilon(1S)(\to K^+K^-\gamma)) = 0.241 \pm 0.001$ and $\epsilon(\Upsilon(3S) \to \pi^+\pi^-\Upsilon(1S)(\to K^+K^-\gamma)) = 0.248 \pm 0.001$. Figure 10 shows the efficiency distributions in the $(m(K^+K^-), \cos\theta_H)$ plane for the $\Upsilon(2S)$ and $\Upsilon(3S)$ data sets.

We also compute the efficiency in the $(\cos\theta_H, \cos\theta_\gamma)$ plane for each considered resonance decaying to $\pi^+\pi^-$ and K^+K^-. Since there are no correlations between these two variables, we parametrize the efficiency as

$$\epsilon(\cos\theta_H, \cos\theta_\gamma) = \epsilon(\cos\theta_H) \times \epsilon(\cos\theta_\gamma). \quad (14)$$

The distributions of the efficiencies as functions of $\cos\theta_H$ and $\cos\theta_\gamma$ are shown in Fig. 11 for the $f_2(1270) \to \pi^+\pi^-$ and $f_2'(1525) \to K^+K^-$ mass regions, for the $\Upsilon(2S)$ data sets. To smoothen statistical fluctuations, the efficiency projections are fitted using seventh- and fourth-order polynomials, respectively. Similar behavior is observed for the other resonances and for the $\Upsilon(3S)$ data sets.

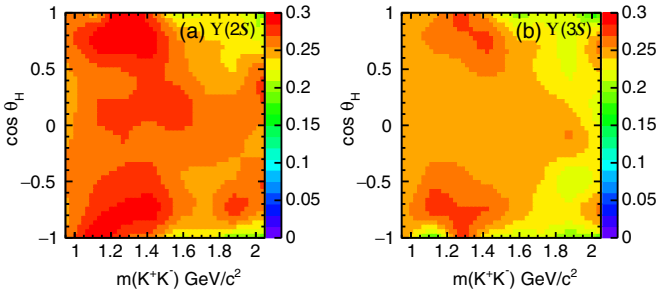

FIG. 10. Fitted efficiency distribution in the $(m(K^+K^-), \cos\theta_H)$ plane for $\Upsilon(1S) \to \gamma K^+K^-$ for the (a) $\Upsilon(2S)$ and (b) $\Upsilon(3S)$ data sets.

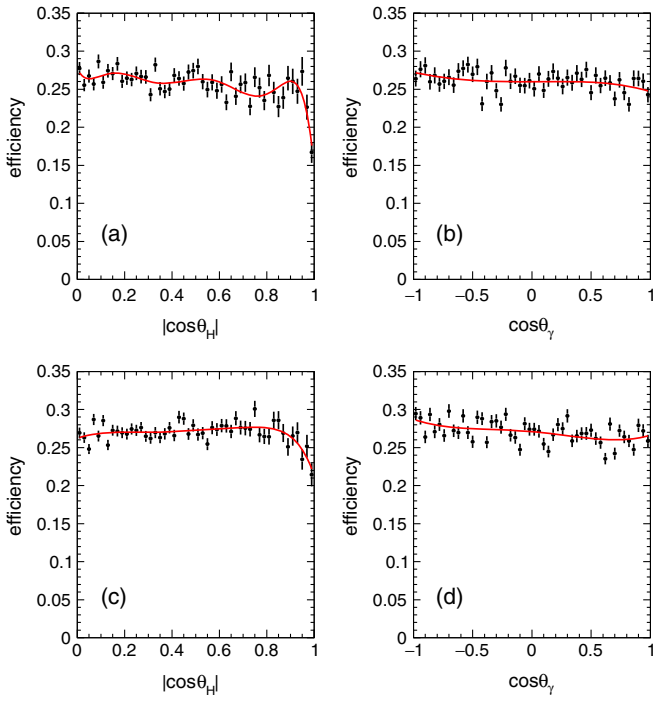

FIG. 11. Efficiency as a function of (a) $\cos\theta_H$ and (b) $\cos\theta_\gamma$ for $\Upsilon(2S) \to \pi_s^+\pi_s^-\Upsilon(1S) \to \gamma f_2(1270)(\to \pi^+\pi^-)$. Efficiency as a function of (c) $\cos\theta_H$ and (d) $\cos\theta_\gamma$ for $\Upsilon(2S) \to \pi_s^+\pi_s^-\Upsilon(1S) \to \gamma f_2'(1525)(\to K^+K^-)$. The lines are the result of the polynomial fits.

B. Efficiency correction

To obtain the efficiency correction weight w_R for the resonance R, we divide each event by the efficiency $\epsilon(\cos\theta_H, \cos\theta_\gamma)$,

$$w_R = \frac{\sum_{i=1}^{N_R} 1/\epsilon_i(\cos\theta_H, \cos\theta_\gamma)}{N_R}, \tag{15}$$

where N_R is the number of events in the resonance mass range. The resulting efficiency weight for each resonance is reported in Table II. We compute separately the $\Upsilon(2S)$ and $\Upsilon(3S)$ yields for resonances decaying to $\pi^+\pi^-$ while, due to the limited statistics, for resonances decaying to K^+K^- the two data sets are merged and corrected using the weighted average efficiency. The systematic effect related to the effect of particle identification is assessed by the use of high statistics control samples. We assign systematic uncertainties of 0.2% to the identification of each pion and 1.0% to that of each kaon. We include an efficiency correction of 0.9885 ± 0.0065 to the reconstruction of the high energy photon, obtained from studies on Data/MC detection efficiency. The efficiency correction contribution due to the limited MC statistics is included using the statistical uncertainty on the average efficiency weight as well as the effect of the fitting procedure. The above effects are added in quadrature and are presented in Table II as systematic uncertainties related to the efficiency correction weight. Finally, we propagate the systematic effect on event yields obtained from the fits to the mass spectra. The resulting efficiency corrected yields are reported in Table II.

VI. LEGENDRE POLYNOMIAL MOMENTS ANALYSIS

To obtain information on the angular momentum structure of the $\pi^+\pi^-$ and K^+K^- systems in $\Upsilon(1S) \to \gamma h^+h^-$, we study the dependence of the $m(h^+h^-)$ mass on the helicity angle θ_H. Figure 12 shows the scatter plot $\cos\theta_H$ vs $m(\pi^+\pi^-)$ for the combined $\Upsilon(2S)$ and $\Upsilon(3S)$ data sets. We observe the spin 2 structure of the $f_2(1270)$.

A better way to observe angular effects is to plot the $\pi^+\pi^-$ mass spectrum weighted by the Legendre polynomial moments, corrected for efficiency. In a simplified environment, the moments are related to the spin 0 (S) and spin 2 (D) amplitudes by the equations [30]:

$$\begin{aligned}\sqrt{4\pi}\langle Y_0^0\rangle &= S^2 + D^2,\\ \sqrt{4\pi}\langle Y_2^0\rangle &= 2SD\cos\phi_{SD} + 0.639D^2,\\ \sqrt{4\pi}\langle Y_4^0\rangle &= 0.857D^2,\end{aligned} \tag{16}$$

TABLE II. Efficiency corrections and efficiency corrected yields for each resonance and data set. The symbol $f_J(1500)$ indicates the signal in the 1500 MeV/c^2 mass region. The error on the efficiency weight w_R includes all the systematic uncertainties related to the reconstruction. The events yields are presented with statistical and total systematic uncertainties.

Resonance $\pi^+\pi^-$	$\Upsilon(2S)$ w_R	$\Upsilon(2S)$ corrected yield	$\Upsilon(3S)$ w_R	$\Upsilon(3S)$ corrected yield
S-wave	4.07 ± 0.06	$541 \pm 65 \pm 53$		
$f_2(1270)$	4.09 ± 0.06	$1043 \pm 78 \pm 36$	3.70 ± 0.05	$285 \pm 26 \pm 15$
$f_0(1710)$	3.97 ± 0.17	$95 \pm 32 \pm 24$	3.60 ± 0.08	$22 \pm 29 \pm 11$
Resonance K^+K^-	$\Upsilon(2S)/\Upsilon(3S)$ w_R	$\Upsilon(2S)/\Upsilon(3S)$ corrected yield		
$f_J(1500)$	3.65 ± 0.14	$281 \pm 37 \pm 38$		
$f_0(1710)$	3.96 ± 0.13	$143 \pm 36 \pm 24$		

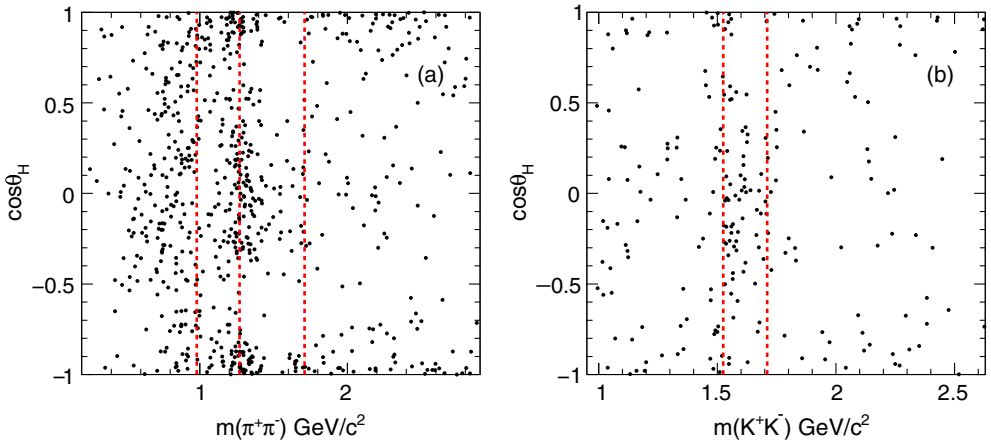

FIG. 12. (a) Uncorrected $\cos\theta_H$ vs $m(\pi^+\pi^-)$ distributions for the combined $\Upsilon(2S)$ and $\Upsilon(3S)$ data sets. The vertical dashed (red) lines indicate the positions of $f_0(980)$, $f_2(1270)$, and $f_0(1710)$. (b) $\cos\theta_H$ vs $m(K^+K^-)$ for the combined $\Upsilon(2S)$ and $\Upsilon(3S)$ data sets. The vertical dashed (red) lines indicate the positions of the $f_2'(1525)$ and $f_0(1710)$.

where ϕ_{SD} is the relative phase. Therefore, we expect to observe spin 2 resonances in $\langle Y_4^0\rangle$ and S/D interference in $\langle Y_2^0\rangle$. The results are shown in Fig. 13. We clearly observe the $f_2(1270)$ resonance in $\langle Y_4^0\rangle$ and a sharp drop in $\langle Y_2^0\rangle$ at the $f_2(1270)$ mass, indicating the interference effect. The distribution of $\langle Y_0^0\rangle$ is just the scaled $\pi^+\pi^-$ mass distribution, corrected for efficiency. Odd L moments are sensitive to the $\cos\theta_H$ forward-backward asymmetry and show weak activity at the position of the $f_2(1270)$ mass. Higher moments are all consistent with zero.

Similarly, we plot in Fig. 14 the K^+K^- mass spectrum weighted by the Legendre polynomial moments, corrected for efficiency. We observe signals of the $f_2'(1525)$ and $f_0(1710)$ in $\langle Y_4^0\rangle$ and activity due to S/D interference effects in the $\langle Y_2^0\rangle$ moment. Higher moments are all consistent with zero.

Resonance angular distributions in radiative $\Upsilon(1S)$ decays from $\Upsilon(2S)/\Upsilon(3S)$ decays are rather complex and will be studied in Sec. VIII. In this section, we perform a simplified partial wave analysis (PWA) solving directly the system of Eq. (16). Figures 15 and 16 show the resulting S-wave and

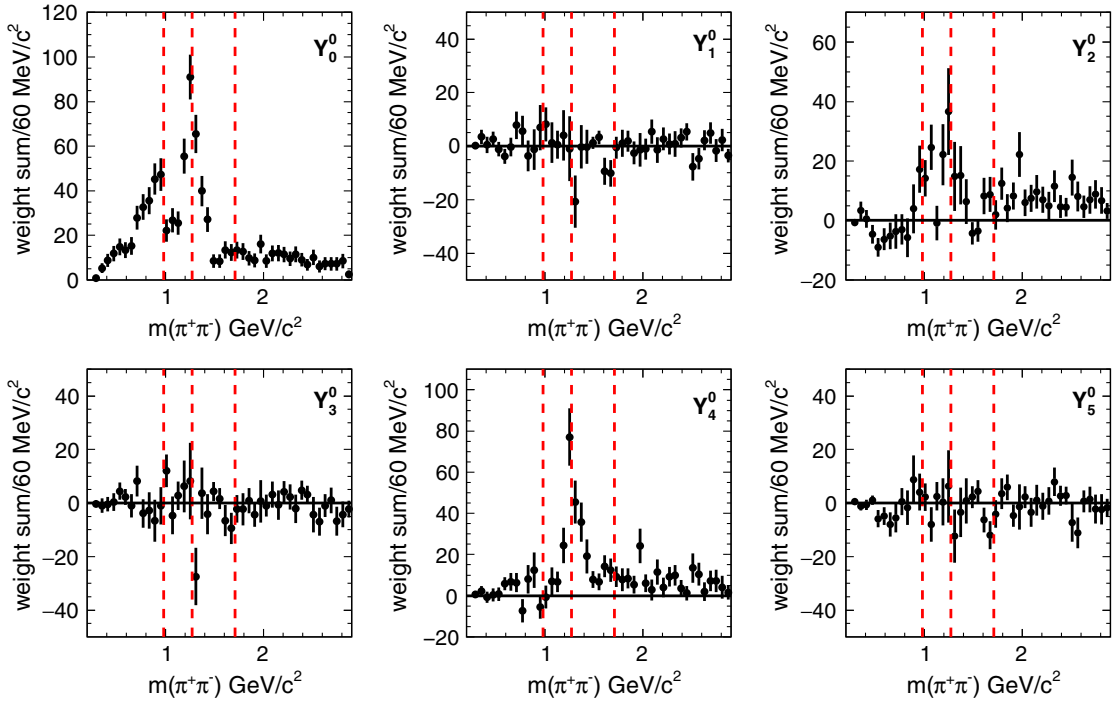

FIG. 13. The distributions of the unnormalized Y_L^0 moments for $\Upsilon(1S)\to\gamma\pi^+\pi^-$ as functions of the $\pi^+\pi^-$ mass corrected for efficiency. The lines indicate the positions of $f_0(980)$, $f_2(1270)$, and $f_0(1710)$.

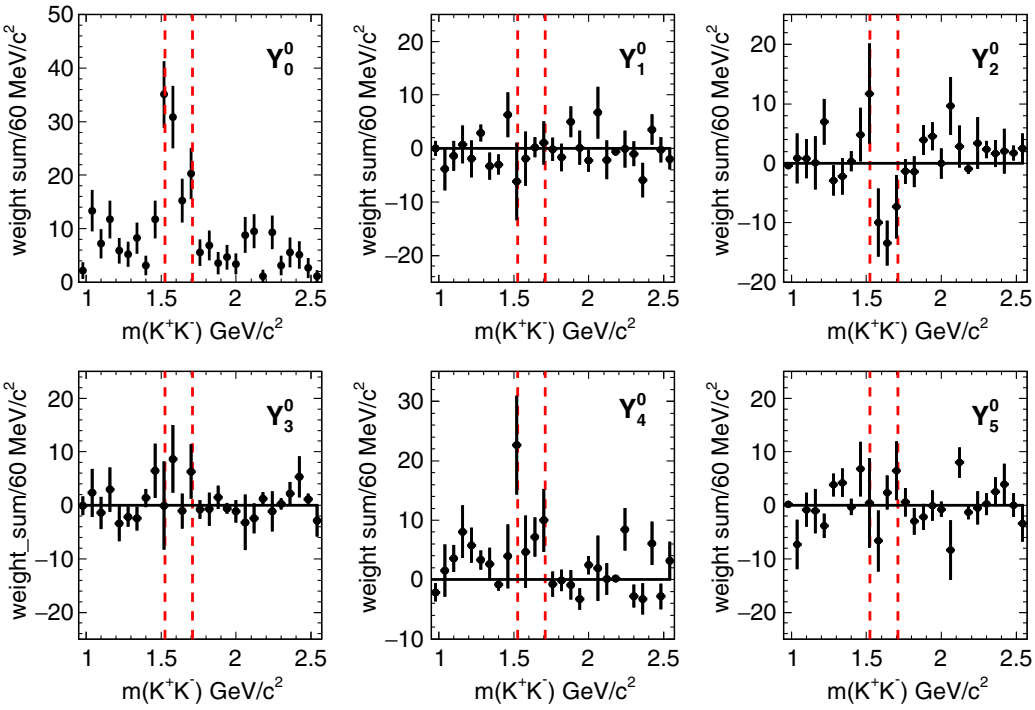

FIG. 14. The distributions of the unnormalized Y^0_L moments for $\Upsilon(1S) \to \gamma K^+K^-$ corrected for efficiency. The lines indicate the positions of the $f_2'(1525)$ and $f_0(1710)$.

D-wave contributions to the $\pi^+\pi^-$ and K^+K^- mass spectra, respectively. Due to the presence of background in the threshold region, the $\pi^+\pi^-$ analysis is performed only on the $\Upsilon(2S)$ data. The relative ϕ_{SD} phase is not plotted because it is affected by very large statistical errors.

We note that in the case of the $\pi^+\pi^-$ mass spectrum we obtain a good separation between S- and D-waves, with the presence of an $f_0(980)$ resonance on top of a broad $f_0(500)$ resonance in the S-wave and a clean $f_2(1270)$ in the D-wave distribution. Integrating the S-wave amplitude from threshold up to a mass of 1.5 GeV/c^2, we obtain an integrated, efficiency corrected yield,

$$N(S-\text{wave}) = 629 \pm 128. \tag{17}$$

in agreement with the results from the fit to the $\pi^+\pi^-$ mass spectrum (see Table II). We also compute the fraction of S-wave contribution in the $f_2(1270)$ mass region defined in Table III and obtain $f_S(\pi^+\pi^-) = 0.16 \pm 0.02$.

In the case of the K^+K^- PWA, the structure peaking around 1500 MeV/c^2 appears in both S- and D-waves suggesting the presence of $f_0(1500)$ and $f_2'(1525)$. In the $f_0(1710)$ mass region, there is not enough data to discriminate between the two different spin assignments. This pattern is similar to that observed in the Dalitz plot analysis of charmless $B \to 3K$ decays [31]. Integrating the S- and

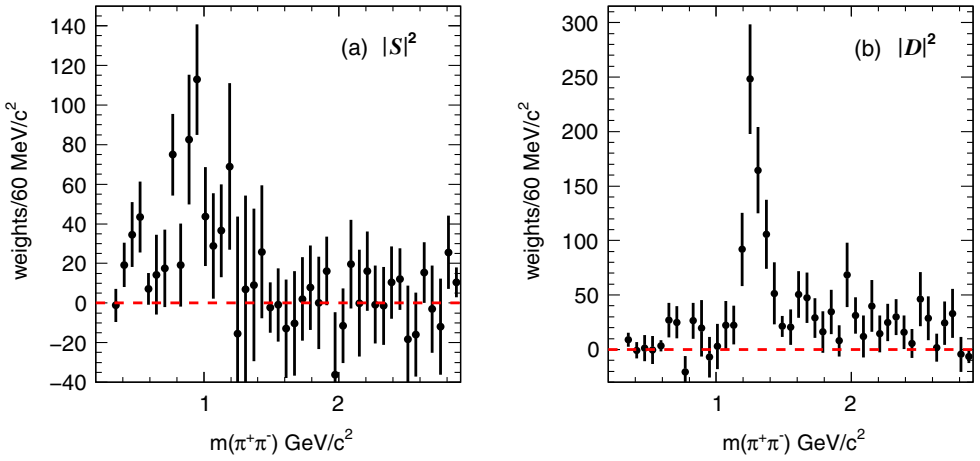

FIG. 15. Results from the simple PWA of the $\pi^+\pi^-$ mass spectrum for the $\Upsilon(2S)$ data. (a) S- and (b) D-wave contributions.

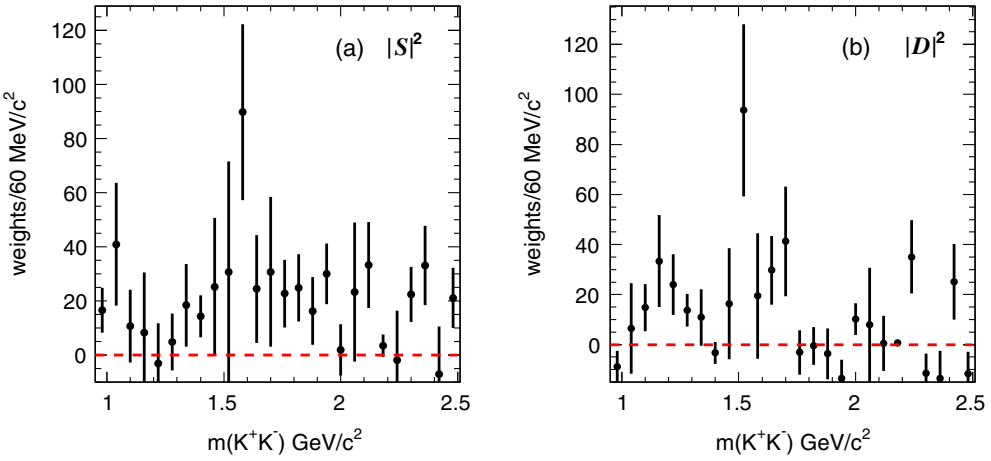

FIG. 16. Results from the simple PWA of the K^+K^- mass spectrum for the combined $\Upsilon(2S)/\Upsilon(3S)$ data. (a) S- and (b) D-wave contributions.

D-wave contributions in the $f_2'(1525)/f_0(1500)$ mass region in the range given in Table III, we obtain a fraction of S-wave contribution $f_S(K^+K^-) = 0.53 \pm 0.10$.

VII. SPIN-PARITY ANALYSIS

We compute the helicity angle θ_π defined as the angle formed by the π_s^+, in the $\pi_s^+\pi_s^-$ rest frame, with respect to the direction of the $\pi_s^+\pi_s^-$ system in the $\Upsilon(1S)\pi_s^+\pi_s^-$ rest frame. This distribution is shown in Fig. 17 for the $\Upsilon(2S)$ data and $\Upsilon(1S) \to \gamma\pi^+\pi^-$, and is expected to be uniform if $\pi_s^+\pi_s^-$ is an S-wave system. The distribution is consistent with this hypothesis with a p-value of 65%.

The $\Upsilon(nS)$ angular distributions are expressed in terms of θ_γ and θ_H. Due to the decay chain used to isolate the $\Upsilon(1S)$ radiative decays [see Eqs. (1) and (2)], the $\Upsilon(1S)$ can be produced with helicity 0 or 1 and the corresponding amplitudes are labeled as A_{00} and A_{01}, respectively. A spin 2 resonance, on the other hand, can have three helicity states, described by amplitudes C_{10}, C_{11}, and C_{12}. We make use of the helicity formalism [32,33] to derive the angular distribution for a spin 2 resonance:

$$
\begin{aligned}
W_2(\theta_\gamma,\theta_H) = \frac{dU(\theta_\gamma,\theta_H)}{d\cos\theta_\gamma\, d\cos\theta_H} = \frac{15}{1024}|E_{00}|^2[&6|A_{01}|^2(22|C_{10}|^2 + 8|C_{11}|^2 + 9|C_{12}|^2) \\
&+ 2|A_{00}|^2(22|C_{10}|^2 + 24|C_{11}|^2 + 9|C_{12}|^2) + 24(|A_{00}|^2 + 3|A_{01}|^2)(2|C_{10}|^2 - |C_{12}|^2)\cos 2\theta_H \\
&+ 6(|A_{00}|^2(6|C_{10}|^2 - 8|C_{11}|^2 + |C_{12}|^2) + |A_{01}|^2(18|C_{10}|^2 - 8|C_{11}|^2 + 3|C_{12}|^2))\cos 4\theta_H \\
&- 2(|A_{00}|^2 - |A_{01}|^2)\cos 2\theta_\gamma(22|C_{10}|^2 - 24|C_{11}|^2 + 9|C_{12}|^2 + 12(2|C_{10}|^2 - |C_{12}|^2)\cos 2\theta_H \\
&+ 3(6|C_{10}|^2 + 8|C_{11}|^2 + |C_{12}|^2)\cos 4\theta_H)].
\end{aligned} \tag{18}
$$

Ignoring the normalization factor $|E_{00}|^2$, there are two amplitudes describing the $\Upsilon(1S)$ helicity states, which can be reduced to one free parameter by taking the ratio $|A_{01}|^2/|A_{00}|^2$. Similarly, the three amplitudes describing the spin 2 helicity states, can be reduced to two free parameters by taking the ratios $|C_{11}|^2/|C_{10}|^2$ and $|C_{12}|^2/|C_{10}|^2$. We therefore have a total of three free parameters.

TABLE III. Results from the helicity amplitude fits to resonances decaying to $\pi^+\pi^-$ and K^+K^-.

Resonance	Mass range (GeV/c^2)	Events	Spin	χ_H, χ_γ, χ_i^2/ndf	$\lvert A_{00}\rvert^2/\lvert A_{01}\rvert^2$		
$\pi\pi$ S-wave	0.6–1.0	104	0	5.8, 8.4, 14.3/19	0.09 ± 0.33		
					$\lvert A_{01}\rvert^2/\lvert A_{00}\rvert^2$	$\lvert C_{11}\rvert^2/\lvert C_{10}\rvert^2$	$\lvert C_{12}\rvert^2/\lvert C_{10}\rvert^2$
$f_2(1270) \to \pi^+\pi^-$	1.092–1.460	280	2	24.0, 46.0, 70/37	1.07 ± 0.31	0.00 ± 0.03	0.29 ± 0.08
$f_2'(1525) \to K^+K^-$	1.424–1.620	36	2	6.7, 1.8, 8.5/16	47.9 ± 10.8	0.42 ± 0.36	1.43 ± 0.35
$f_0(1500) \to K^+K^-$		40	0		0.04 ± 0.07		

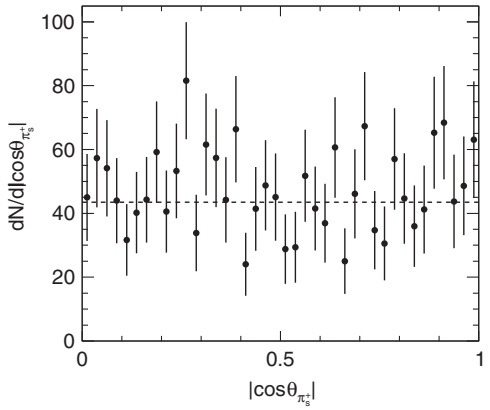

FIG. 17. Efficiency-corrected distribution of θ_π in the $\Upsilon(2S)$ data. The dashed line is the result of a fit to a uniform distribution.

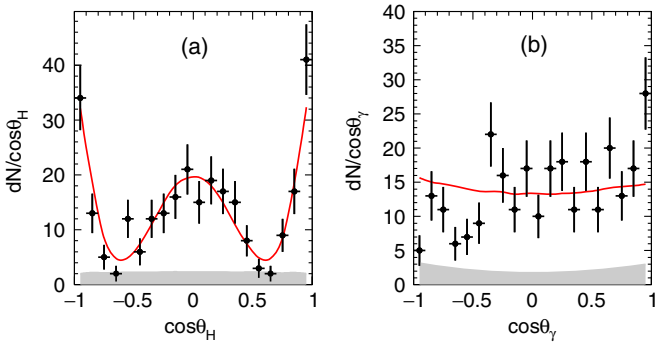

FIG. 18. Uncorrected (a) $\cos\theta_H$ and (b) $\cos\theta_\gamma$ distributions in the $f_2(1270) \to \pi^+\pi^-$ mass region. The full (red) lines are the projections from the fit with the spin 2 hypothesis. The shaded (gray) area represents the S-wave background contribution.

The expected angular distribution for a spin 0 resonance is given by

$$W_0(\theta_\gamma) = \frac{dU(\theta_\gamma)}{d\cos\theta_\gamma} = \frac{3}{8}|C_{10}|^2|E_{00}|^2(|A_{00}|^2 + 3|A_{01}|^2 - (|A_{00}|^2 - |A_{01}|^2)\cos 2\theta_\gamma). \quad (19)$$

Ignoring the normalization factors $|C_{10}|^2$ and $|E_{00}|^2$, the distribution has only one free parameter, $|A_{01}|^2/|A_{00}|^2$.

We perform a two-dimensional unbinned maximum likelihood fit for each resonance region defined in Table III. If N is the number of available events, the likelihood function $\mathcal{L}$ is written as

$$\mathcal{L} = \prod_{n=1}^{N}\left[f_{\rm sig}\frac{\epsilon(\cos\theta_H,\cos\theta_\gamma)W_s(\theta_H,\theta_\gamma)}{\int W_s(\theta_H,\theta_\gamma)\epsilon(\cos\theta_H,\cos\theta_\gamma)d\cos\theta_H d\cos\theta_\gamma} + (1-f_{\rm sig})\frac{\epsilon(\cos\theta_H,\cos\theta_\gamma)W_b(\theta_H,\theta_\gamma)}{\int W_b(\theta_H,\theta_\gamma)\epsilon(\cos\theta_H,\cos\theta_\gamma)d\cos\theta_H d\cos\theta_\gamma}\right], \quad (20)$$

where $f_{\rm sig}$ is the signal fraction, $\epsilon(\cos\theta_H, \cos\theta_\gamma)$ is the fitted efficiency [Eq. (14)], and W_s and W_b are the functions describing signal and background contributions, given by Eq. (18) or Eq. (19). Since the background under the $\pi^+\pi^-$ and K^+K^- mass spectra is negligible in the low-mass regions, we include only the tails of nearby adjacent resonances. In the description of the $\pi^+\pi^-$ data in the threshold region, we make use only of the $\Upsilon(2S)$ data because of the presence of a sizeable $\rho(770)^0$ background in the $\Upsilon(3S)$ sample.

We first fit the $f_2(1270)$ angular distributions and allow a background contribution of 16% (see Sec. VII) from the S-wave having fixed parameters. Therefore an iterative procedure of fitting the S-wave and $f_2(1270)$ regions is performed. Figure 18 shows the uncorrected fit projections on $\cos\theta_H$ and $\cos\theta_\gamma$. The $\cos\theta_\gamma$ spectrum is approximately uniform, while $\cos\theta_H$ shows structures well-fitted by the spin 2 hypothesis. Table III summarizes the results from the fits. We use as figures of merit $\chi_H = \chi^2(\cos\theta_H)$, $\chi_\gamma = \chi^2(\cos\theta_\gamma)$ and their sum $\chi_t^2 = (\chi_H + \chi_\gamma)/\text{ndf}$ computed as the χ^2 values obtained from the $\cos\theta_H$ and $\cos\theta_\gamma$ projections, respectively. We use $\text{ndf} = N_{\rm cells} - N_{\rm par}$, where $N_{\rm par}$ is the number of free parameters in the fit and $N_{\rm cells}$ is the sum of the number of bins along the $\cos\theta_H$ and $\cos\theta_\gamma$ axes. We note a good description of the $\cos\theta_H$ projection but a poor description of the $\cos\theta_\gamma$ projection. This may be due to the possible presence of additional scalar components in the $f_2(1270)$ mass region, not taken into account in the formalism used in this analysis.

We fit the S-wave region in the $\pi^+\pi^-$ mass spectrum from the $\Upsilon(2S)$ decay including as background the spin 2 contribution due to the tail of the $f_2(1270)$. The latter is estimated to contribute with a fraction of 9%, with parameters fixed to those obtained from the $f_2(1270)$ spin analysis described above. Figure 19 shows the fit

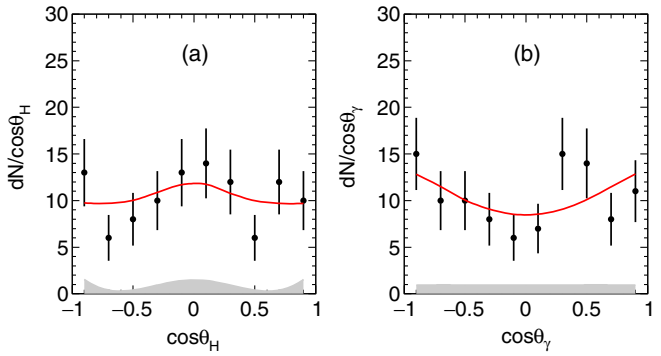

FIG. 19. Uncorrected (a) $\cos\theta_H$ and (b) $\cos\theta_\gamma$ distributions in the S-wave $\to \pi^+\pi^-$ mass region. The full (red) lines are the projections from the fit using the spin 0 hypothesis. The shaded (gray) area represents the background contribution from the $f_2(1270)$.

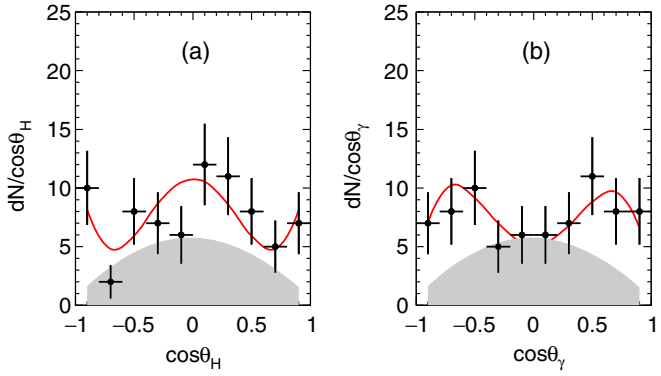

FIG. 20. Uncorrected (a) $\cos\theta_H$ and (b) $\cos\theta_\gamma$ distributions in the $f_J(1500) \to K^+K^-$ mass region. The full (red) lines are the projections from the fit using the superposition of spin-2 and spin-0 hypotheses. The shaded (gray) area represents the spin-0 contribution.

projections on the $\cos\theta_H$ and $\cos\theta_\gamma$ distributions and Table III gives details on the fitted parameters. We obtain a good description of the data consistent with the spin 0 hypothesis.

We fit the K^+K^- data in the $f_J(1500)$ mass region, where many resonances can contribute: $f_2'(1525)$, $f_0(1500)$ [31], and $f_0(1710)$. We fit the data using a superposition of S- and D-waves, having helicity contributions as free parameters, and free S-wave contribution. We obtain an S-wave contribution of $f_S(K^+K^-) = 0.52 \pm 0.14$, in agreement with the estimate obtained in Sec. VI. The helicity contributions are given in Table III and fit projections are shown in Fig. 20, giving an adequate description of the data. We assign the spin-2 contribution to the $f_2'(1525)$ and the spin-0 contribution to the $f_0(1500)$ resonance. We also fit the data assuming the presence of the spin-2 $f_2'(1525)$ only hypothesis. We obtain a likelihood variation of $\Delta(-2\log\mathcal{L}) = 1.3$ for the difference of two parameters between the two fits. Due the low statistics we cannot statistically distinguish between the two hypotheses.

VIII. MEASUREMENT OF BRANCHING FRACTIONS

We determine the branching fraction $\mathcal{B}(R)$ for the decay of $\Upsilon(1S)$ to photon and resonance R using the expression

$$\mathcal{B}(R) = \frac{N_R(\Upsilon(nS) \to \pi_s^+\pi_s^-\Upsilon(1S)(\to R\gamma))}{N(\Upsilon(nS) \to \pi_s^+\pi_s^-\Upsilon(1S)(\to \mu^+\mu^-))} \times \mathcal{B}(\Upsilon(1S) \to \mu^+\mu^-), \quad (21)$$

where N_R indicates the efficiency-corrected yield for the given resonance. To reduce systematic uncertainties, we first compute the relative branching fraction to the reference channel $\Upsilon(nS) \to \pi^+\pi^-\Upsilon(1S)(\to \mu^+\mu^-)$, which has the same number of charged particles as the final states under study. We then multiply the relative branching fraction by the well-measured branching fraction $\mathcal{B}(\Upsilon(1S) \to \mu^+\mu^-) = 2.48 \pm 0.05\%$ [25].

We determine the reference channel corrected yield using the method of "B-counting," also used to obtain the number of produced $\Upsilon(2S)$ and $\Upsilon(3S)$ [22]. Taking into account the known branching fractions of $\Upsilon(2S)/\Upsilon(3S) \to \pi_s^+\pi_s^-\Upsilon(1S)$, we obtain

$$N(\Upsilon(2S) \to \pi_s^+\pi_s^-\Upsilon(1S)(\to \mu^+\mu^-)) = (4.35 \pm 0.12_{\rm sys}) \times 10^5 \quad (22)$$

and

$$N(\Upsilon(3S) \to \pi_s^+\pi_s^-\Upsilon(1S)(\to \mu^+\mu^-)) = (1.32 \pm 0.04_{\rm sys}) \times 10^5 \quad (23)$$

events. As a cross-check, we reconstruct $\Upsilon(nS) \to \pi^+\pi^-\Upsilon(1S)(\to \mu^+\mu^-)$ corrected for efficiency and obtain yields in good agreement with those obtained using the method of "B-counting."

Table IV gives the measured branching fractions. In all cases, we correct the efficiency corrected yields for isospin and for PDG measured branching fractions [25]. In these measurements, the $f_2(1270)$ yield is corrected first for the $\pi^0\pi^0$ (33.3%) and then for the $\pi\pi$ ($84.2^{+2.9}_{-0.9}\%$) branching fractions. We also correct the $\pi\pi$ S-wave and $f_0(1710)$ branching fractions for the $\pi^0\pi^0$ decay mode. In the case of $f_J(1500) \to K^+K^-$, the spin analysis reported in Secs. VI and VII gives indications of the presence of overlapping $f_2'(1525)$ and $f_0(1500)$ contributions. We give the branching fraction for $f_J(1500) \to K^+K^-$ and, separately, for the $f_2'(1525)$ and $f_0(1500)$, where we make use of the S-wave contribution $f_S(K^+K^-) = 0.52 \pm 0.14$, obtained in Sec. VII.

The $f_2'(1525)$ branching fraction is corrected for the $K\bar{K}$ decay mode ($(88.7 \pm 2.2)\%$). For all the resonances decaying to $K\bar{K}$, the branching fractions are corrected for the unseen $K^0\bar{K}^0$ decay mode (50%).

For the $f_2(1270)$ and $f_0(1710)$ resonances decaying to $\pi^+\pi^-$, the relative branching ratios are computed separately for the $\Upsilon(2S)$ and $\Upsilon(3S)$ data sets, obtaining good

TABLE IV. Measured $\Upsilon(1S) \to \gamma R$ branching fractions.

Resonance	$\mathcal{B}$ (10^{-5})
$\pi\pi$ S-wave	$4.63 \pm 0.56 \pm 0.48$
$f_2(1270)$	$10.15 \pm 0.59^{+0.54}_{-0.43}$
$f_0(1710) \to \pi\pi$	$0.79 \pm 0.26 \pm 0.17$
$f_J(1500) \to K\bar{K}$	$3.97 \pm 0.52 \pm 0.55$
$f_2'(1525)$	$2.13 \pm 0.28 \pm 0.72$
$f_0(1500) \to K\bar{K}$	$2.08 \pm 0.27 \pm 0.65$
$f_0(1710) \to K\bar{K}$	$2.02 \pm 0.51 \pm 0.35$

agreement. The values reported in Table IV are determined using the weighted mean of the two measurements.

Since the reference channel has the same number of tracks as the final state, systematic uncertainties related to tracking are negligible with respect to the errors due to other sources. The systematic uncertainty related to the "*B*-counting" estimate of the event yields in the denominator of Eq. (21) is propagated into the total systematic uncertainty on the branching fractions given in Table IV.

Comparing with CLEO results, we note that our results on the *S*-wave contribution include the $f_0(980)$ and $f_0(500)$ contributions, while the CLEO analysis determines the branching fraction for the peaking structure at the $f_0(980)$ mass. In the same way, a direct comparison for the $f_2'(1525)$ branching fraction is not possible due to the $f_0(1500)$ contribution included in the present analysis. The branching fraction for the $f_2(1270)$ is in good agreement.

We report the first observation of $f_0(1710)$ in $\Upsilon(1S)$ radiative decay with a significance of 5.7σ, combining $\pi^+\pi^-$ and K^+K^- data. To determine the branching ratio of the $f_0(1710)$ decays to $\pi\pi$ and $K\bar{K}$, we remove all the systematic uncertainties related to the reference channels and of the γ reconstruction. Labeling with N the efficiency-corrected yields for the two $f_0(1710)$ decay modes, we obtain

$$\frac{\mathcal{B}(f_0(1710)\to\pi\pi)}{\mathcal{B}(f_0(1710)\to K\bar{K})}=\frac{N(f_0(1710)\to\pi\pi)}{N(f_0(1710)\to K\bar{K})}=0.64\pm0.27_{\rm stat}\pm0.18_{\rm sys}, \quad (24)$$

in agreement with the world average value of $0.41^{+0.11}_{-0.17}$ [25].

IX. SUMMARY

We have studied the $\Upsilon(1S)$ radiative decays to $\gamma\pi^+\pi^-$ and γK^+K^- using data recorded with the *BABAR* detector operating at the SLAC PEP-II asymmetric-energy e^+e^- collider at center-of-mass energies at the $\Upsilon(2S)$ and $\Upsilon(3S)$ resonances, using integrated luminosities of 13.6 fb^{-1} and 28.0 fb^{-1}, respectively. The $\Upsilon(1S)$ resonance is reconstructed from the decay chains $\Upsilon(nS)\to\pi^+\pi^-\Upsilon(1S)$, $n=2,3$. Spin-parity analyses and branching fraction measurements are reported for the resonances observed in the $\pi^+\pi^-$ and K^+K^- mass spectra. In particular, we report the observation of broad *S*-wave, $f_0(980)$, and $f_2(1270)$ resonances in the $\pi^+\pi^-$ mass spectrum. We observe a signal in the 1500 MeV/c^2 mass region of the K^+K^- mass spectrum for which the spin analysis indicates contributions from both $f_2'(1525)$ and $f_0(1500)$ resonances. We also report observation of $f_0(1710)$ in both $\pi^+\pi^-$ and K^+K^- mass spectra, with combined significance of 5.7σ, and measure the relative branching fraction. These results may contribute to the long-standing issue of the identification of a scalar glueball.

Reference [3] reports on a detailed discussion on the status of the search for the scalar glueball, listing as candidates the broad $f_0(500)$, $f_0(1370)$, $f_0(1500)$, and $f_0(1710)$. For this latter state, in the gluonium hypothesis, Ref. [10] computes a branching fraction of $\mathcal{B}(\Upsilon(1S)\to\gamma f_0(1710))=0.96^{+0.55}_{-0.23}\times10^{-4}$. Taking into account the presence of additional, not well measured, $f_0(1710)$ decay modes, our result is consistent with this predicted branching fraction as well as with the dominance of an $s\bar{s}$ decay mode. For $f_0(1500)\to K\bar{K}$, Ref. [13] expects a branching fraction $\mathcal{B}(\Upsilon(1S)\to\gamma f_0(1500))$ in the range $2\sim4\times10^{-5}$, consistent with our measurement. The status of $f_0(1370)$ is controversial [34] as this state could just be an effect related to the broad $f_0(500)$. Reference [10] estimates for $f_0(1370)$ a branching fraction of $\mathcal{B}(\Upsilon(1S)\to\gamma f_0(1370))=3.2^{+1.8}_{-0.8}\times10^{-5}$, in the range of our measurement of the branching fraction of $\mathcal{B}(\Upsilon(1S)\to\gamma(\pi\pi S\text{-wave}))$.

ACKNOWLEDGMENTS

We are grateful for the extraordinary contributions of our PEP-II2 colleagues in achieving the excellent luminosity and machine conditions that have made this work possible. The success of this project also relies critically on the expertise and dedication of the computing organizations that support *BABAR*. The collaborating institutions wish to thank SLAC for its support and the kind hospitality extended to them. This work is supported by the U.S. Department of Energy and National Science Foundation, the Natural Sciences and Engineering Research Council (Canada), the Commissariat à l'Energie Atomique and Institut National de Physique Nucléaire et de Physique des Particules (France), the Bundesministerium für Bildung und Forschung and Deutsche Forschungsgemeinschaft (Germany), the Istituto Nazionale di Fisica Nucleare (Italy), the Foundation for Fundamental Research on Matter (The Netherlands), the Research Council of Norway, the Ministry of Education and Science of the Russian Federation, Ministerio de Economia y Competitividad (Spain), and the Science and Technology Facilities Council (United Kingdom). Individuals have received support from the Marie-Curie IEF program (European Union), the A. P. Sloan Foundation (USA), and the Binational Science Foundation (USA-Israel). We acknowledge P. Colangelo for useful suggestions.

[1] Y. Chen *et al.*, Phys. Rev. D **73**, 014516 (2006).
[2] E. Klempt and A. Zaitsev, Phys. Rep. **454**, 1 (2007).
[3] W. Ochs, J. Phys. G **40**, 043001 (2013).
[4] P. Minkowski and W. Ochs, Eur. Phys. J. C **9**, 283 (1999).
[5] C. Amsler and F. E. Close, Phys. Lett. B **353**, 385 (1995).
[6] C. Amsler and F. E. Close, Phys. Rev. D **53**, 295 (1996).
[7] S. Janowski, F. Giacosa, and D. H. Rischke, Phys. Rev. D **90**, 114005 (2014).
[8] M. Chanowitz, Phys. Rev. Lett. **95**, 172001 (2005).
[9] K.-T. Chao, X. G. He, and J. P. Ma, Phys. Rev. Lett. **98**, 149103 (2007).
[10] R. Zhu, J. High Energy Phys. 09 (2015) 166.
[11] S. Fleming and A. K. Leibovich, Phys. Rev. D **70**, 094016 (2004).
[12] S. Fleming, C. Lee, and A. K. Leibovich, Phys. Rev. D **71**, 074002 (2005).
[13] X. G. He, H. Y. Jin, and J. P. Ma, Phys. Rev. D **66**, 074015 (2002).
[14] L. Köpke and N. Wermes, Phys. Rep. **174**, 67 (1989).
[15] J. Z. Bai *et al.* (BES Collaboration), Phys. Rev. Lett. **77**, 3959 (1996).
[16] J. Z. Bai *et al.* (BES Collaboration), Phys. Rev. D **67**, 032004 (2003).
[17] S. B. Athar *et al.* (CLEO Collaboration), Phys. Rev. D **73**, 032001 (2006).
[18] D. Besson *et al.* (CLEO Collaboration), Phys. Rev. D **75**, 072001 (2007).
[19] J. P. Lees *et al.* (*BABAR* Collaboration), Nucl. Instrum. Methods Phys. Res., Sect. A **726**, 203 (2013).
[20] B. Aubert *et al.* (*BABAR* Collaboration), Nucl. Instrum. Methods Phys. Res., Sect. A **479**, 1 (2002); **729**, 615 (2013).
[21] S. Agostinelli *et al.* (Geant4 Collaboration), Nucl. Instrum. Methods Phys. Res., Sect. A **506**, 250 (2003); D. J. Lange, Nucl. Instrum. Methods Phys. Res., Sect. A **462**, 152 (2001).
[22] Ed. A. J. Bevan, B. Golob, Th. Mannel, S. Prell, and B. D. Yabsley, Eur. Phys. J. C **74**, 3026 (2014).
[23] S. M. Flatté, Phys. Lett. B **63**, 224 (1976).
[24] T. A. Armstrong *et al.* (WA76 Collaboration), Z. Phys. C **51**, 351 (1991).
[25] C. Patrignani *et al.* (Particle Data Group), Chin. Phys. C **40**, 100001 (2016).
[26] S. Dobbs, A. Tomaradze, T. Xiao, and K. K. Seth, Phys. Rev. D **91**, 052006 (2015).
[27] J. Blatt and V. Weisskopf, *Theoretical Nuclear Physics* (Wiley, New York, 1952).
[28] R. M. Baltrusaitis *et al.* (Mark III Collaboration), Phys. Rev. D **35**, 2077 (1987).
[29] C. De Boor, *A Practical Guide to Splines* (Springer, New York, 2001).
[30] G. Costa *et al.* Nucl. Phys. **B175**, 402 (1980).
[31] J. P. Lees *et al.* (*BABAR* Collaboration), Phys. Rev. D **85**, 112010 (2012).
[32] L. Breva-Newell, Decays of the $\Upsilon(1S)$ into a photon and two charged hadrons, Ph.D. thesis, 2004, arXiv:hep-ex/0412075.
[33] J. D. Richman, An experimenter's guide to the helicity formalism, California Institute of Technology, Report No. CALT-68-1148 (1984).
[34] W. M. Yao *et al.* (Particle Data Group), J. Phys. G **33**, 1 (2006).